Effect of Constraint on Ductile Crack Growth and Ductile-Brittle Fracture Transition of a carbon Steel

C. Yan* and Y.W. Mai

Centre of Advanced Materials Technology, Mechanical & Mechatronic Department, The University of Sydney, NSW 2006, Australia

Abstract. Ductile-brittle fracture transition was investigated using compact tension (CT) specimens from -70^{o}C to 40^{o}C for a carbon steel. Large deformation finite element analysis has been carried out to simulate the stable crack growth in the compact tension (CT, a/W=0.6), three point-point bend (SE(B), a/W=0.1) and centre-cracked tension (M(T), a/W=0.5) specimens. Experimental crack tip opening displacement (CTOD) resistance curve was employed as the crack growth criterion. Ductile tearing is sensitive to constraint and tearing modulus increases with reduced constraint level. The finite element analysis shows that path-dependence of J-integral occurs from the very beginning of crack growth and ductile crack growth elevates the opening stress on the remaining ligament. Cleavage may occur after some ductile crack growth due to the increase of opening stress. For both stationary and growing cracks, the magnitude of opening stress increases with increasing in-plane constraint. The ductile-brittle transition takes place when the opening stress ahead of the crack tip reaches the local cleavage stress as the in-plane constraint of the specimen increases.

---

* To whom all the correspondence should be addressed.

Fax: 61-2-93517060
E-mail: ycheng@ tiny.me.su.oz.au

1. Introduction

The phenomenon of ductile-brittle fracture transition has been observed in low and medium carbon steels [1-2]. Decreasing test temperature and increasing loading rate can prompt the ductile-brittle transition, which can be explained in terms of the elevated yield stress of the material. Also, ductile-brittle transition can occur as a result of a transition from plane stress fracture for a thin plate to plane strain fracture for a thick plate in which the high hydrostatic stress elevates the opening stress ahead of the crack tip. In the work of Wu, Mai and Cotterell [3], notched-bend specimen of a medium carbon steel had a ductile-brittle transition with increasing the normalized crack length. Their finite element analysis indicated that the opening stress ahead of a shallow crack is less than that of a deep crack due to the lower in-plane constraint.

Recently, O'Dowd and Shih [4-5] have shown that for a full range of plastic constraint the stress field of the forward sector of the crack tip can be characterized by the two parameter J and Q. The J-integral characterize the intensity of the HRR stress and Q represents the stress triaxiality or constraint. By incorporating a micromechanical model for cleavage fracture, e.g., the work of Ritchie et al [6], the variation of cleavage toughness with constraint has been predicted for different specimen geometry [7]. However, the stress fields ahead of a growing crack is different from stationary crack. It is uncertain whether J-Q theory can be used to predict toughness variation in ductile-brittle transition region. The finite element analysis of Varias and Shih [8] showed that the in-plane constraint has an influence on the stress fields ahead of a steady growing crack under small scale yield condition. The work of Xia and Shih [9] and Ruggieri and Dodds [10] also indicated that the initial crack length affects the stress field ahead of a growing crack.

In the present study, compact tension (CT, a/W=0.6) specimens for a carbon steel were tested from -70^{o}C to 40^{o}C. At 30^{o}C, three-point bend specimen (SE(B), a/W=0.1) and centre-cracked panel specimen (M(T), a/W=0.5) have been tested by Wu and Mai [11] for the same material. Large deformation finite element analysis is undertaken to simulate stable crack growth for the above three types of specimens. The effect of constraint on crack growth resistance curve and ductile-brittle fracture transition has been examined.

2. Experimental procedure

The material used for the experiments was a carbon steel whose chemical composition is given in Table 1. Its yield strength (σ_o) and hardening exponent (n) obtained from round bar tensile specimens are listed in Table 2. The true stress-true strain relation can be presented by

$$\sigma = K\varepsilon^n \qquad (1)$$

where K is a constant and their values are also given in Table 2. Standard 1T compact tension (CT) specimens with an a/W ratio 0.6 were used to measure the fracture toughness at -70^{o}C, -40^{o}C, -30^{o}C, -20^{o}C, -10^{o}C, 0^{o}C, 10^{o}C, 20^{o}C, 30^{o}C and 40^{o}C. Crack tip opening displacement (CTOD) at unstable fracture (δ_c) was obtained according to ASTM standard E1290-93 then δ_c was corrected for crack growth in terms of the equation proposed by Hellmann and Schwalbe's equation [12]

$$\delta = \frac{K^2(1-\nu^2)}{2\sigma_o E} + \frac{[r_p(W-a)+\Delta a]V_p}{[r_p(W-a)+a+Z]} \qquad (2)$$

where K is the nominal stress-intensity factor, E is the Young's modulus, ν is the Poisson's ratio, V_p is the plastic component of the crack-mouth opening displacement at the unstable point on the load-displacement record, Z is the distance of knife edge measurement point from the front face of specimen, the r_p is the plastic rotation factor. CTOD at ductile initiation, δ_i, was obtained by multi-specimen resistance curve (δ_R-curve) method at 30^{o}C.

All tests were carried out in Instron 1195 testing machine with a crosshead speed of 1.0mm/min. The test temperature were controlled using a close-loop constant temperature chamber. The fracture surface of CT specimens fractured at -70^{o}C and -30^{o}C were observed using scanning electron microscope (SEM). The distance (X_f) from the cleavage initiation site to the blunted crack tip for the specimens with complete cleavage or to the growing crack tip for the specimens with cleavage preceded by ductile growth were measured. Wu and Mai [11] have measured δ_R-curves for the same material using three point-point bend (SE(B), a/W=0.1), and centre-cracked tension (M(T), a/W=0.5) specimens at 30^{o}C. The configuration of all specimens are shown in Fig. 1.

3. Finite element analysis procedure

Large deformation finite element analysis is carried out using ABAQUS code [13]. An incremental plasticity theory was used for the material constitutive model. The yield function *f* is related to uniaxial tension by

$$f(\boldsymbol{\sigma}) = \overline{\sigma}(\varepsilon^{p}) \qquad (3)$$

where ε^{p} is the plastic strain and $\boldsymbol{\sigma}$ and $\overline{\sigma}$ are the Cauchy (true) stress and equivalent (uniaxial) stress respectively. The form of *f* employed in this study is the Von Mises yield function

$$f(\boldsymbol{\sigma}) = \left(\frac{3}{2}(\mathbf{s}_{ij}\mathbf{s}_{ij})\right)^{1/2} \qquad (4)$$

where $\mathbf{S}_{ij}$ is the deviatoric component of stress.

According to the specimen dimensions shown in Fig. 1, different finite element meshes were applied for various specimens. Fig. 2 shows the details of the mesh near to the initial crack tip. Four node quadratic elements are placed in the crack plane to simulate the crack growth, which have the width of 0.1 mm along the crack line. The crack growth was simulated by the node release technique incorporated in the ABAQUS code. The crack growth starts when the original crack tip reaches the initiation CTOD, i.e., δ_i. The crack growth then follows δ_R-curve. The validity of this method has been proven by some researches [14-15]. Also, the J-integral was evaluated according to domain integral method. The integral contours were taken trough the centroids of rings of elements surrounding the crack tip as shown in Fig. 2. A total of 12 J-integral were calculated for each case but results are only reported for number 1, 5, 10, and 12, i.e., J_1, J_5, J_{10} and J_{12}.

4. Results and discussion

4.1 crack growth resistance curves

Fig. 3 shows the load-load line displacement curve for CT specimen from finite element simulation together with the experimental record. A good agreement can be found between the two curves. This further verified the validity of the finite element simulation. Fig. 4 shows the experimental δ_R-curve for CT, SE(B) and M(T) specimens. The specimen geometry has an effect on the δ_R-curve resistance curve. The tearing modulus for the CT specimen is apparently lower than that for the SE(B) and M(T) specimens. J_R-curve can be obtained from bend-type specimens by standard procedure [16]. J-integral is path independent for a stationary crack under the deformation theory of plasticity [17-18]. After ductile crack growth, Hutchinson and Paris [19] pointed out that J can still control crack growth when some conditions are met. Firstly, the crack growth (Δa) should be small compared to the remaining ligament b,

$$\Delta a << b \qquad (5)$$

In ASTM standard E1152-95 [16], this condition is restated as

$$\frac{\Delta a}{b_o} < 0.10 \qquad (6)$$

where b_o is the original ligament. Secondly, the following inequality should be satisfied for J controlled crack growth,

$$\omega \equiv \frac{b}{J}\frac{dJ}{da} > 10 \qquad (7)$$

C.F. Shih et al [20] presented another condition for J-controlled crack extension,

$$B, b > \frac{20J}{\sigma_o} \qquad (8)$$

where B is the thickness of specimen.

The results of G. P. Gibson et al [21] have questioned above limitations. Testing of different specimen geometry and loading conditions revealed a considerable difference in the J_R-curve [22-25]. For CT specimen, some numerical analysis [14,26] indicated the J is path-dependent at the beginning of crack growth. In Fig. 5, for CT specimens, the calculated J-integral is path-dependent at the very beginning of crack growth. Similar phenomenon can be observed for SE(B) and M(T) specimens. Table. 3 indicates the parameters related to the restrictions for J controlled crack growth (equations 6, 7, and 8) for CT and SE(B) specimens. In Table 3, when crack extension Δa=0.3 mm for CT and Δa=0.1 mm for SE(B) specimens, the limit $b\sigma_o/J$ (equation 8) is first reached before other limits ($\Delta a/b_o$ and ω). This is consistent with the result of Xin et al [26].

Fig. 6 indicates the variation of crack tip opening angle (CTOA) for CT, SE(B) and M(T) specimens. It is apparent that CTOA keeps almost constant except at the beginning of crack growth. The CTOA for CT specimen is smaller than that for SE(B) and M(T) specimens.

In summary, the specimen geometry has an effect on δ_R-curve and CTOA during crack growth. J-integral is path-dependent at very beginning of crack growth.

4.2 Stress and strain distributions ahead of a growing crack

Fig. 7(a) shows the opening stress σ_{22}/σ_o ahead of crack tip before and after ductile crack growth in CT, M(T) and SE(B) specimens (Δa=1.0mm). It is clear that opening stress increases after ductile crack growth. The position of peak opening stress shifts to crack tip with crack growth. For both the stationary and growing cracks, the peak opening stress ahead of the crack tip increases in the order of CT, SE(B) and M(T) specimens. Fig. 7(b) shows the distribution of stress triaxiality ahead of the growing crack tip. The stress triaxiality is expressed as the ratio of the hydrostatic stress σ_m over the Von Mises effective stress σ_e. The CT specimen has the highest stress triaxiality, i.e., highest constraint level and M(T) has the lowest. Fig. 8 shows the variation of peak opening stress with crack growth. It can be seen that the peak opening stress increases after the onset of ductile crack growth. After certain amount of growth (about 1.0mm), peak σ_{22} remains almost constant. Fig. 9 illustrate the distributions of effective plastic strain ahead of crack tip at various stages of crack growth for CT specimen. The effective plastic strain ahead of a growing crack falls significantly below the distribution for stationary crack. The same trend can be found in SE(B) and M(T) specimens. It is consistent with the numerical calculation of Sattar-Far [27]. The experimental research [28] also indicated that the strain singularity in front of a growing crack is lower than that for a stationary crack.

4.3 Ductile-brittle fracture transition

In the present study, the variation of δ_c in CT specimens with temperature is shown in Fig. 10. At -70^{o}C and -40^{o}C, fracture occurred as complete cleavage without any ductile growth. At -30^{o}C, -20^{o}C, -10^{o}C and 0^{o}C, some specimens were cleavage without ductile

growth; but in some specimens cleavage was preceded by ductile growth. From 10^oC to 30^oC, all CT specimens cleavage after some ductile growth. Above 30^oC, fracture was dominated by whole ductile tearing. For SE(B) and M(T) specimens at 30^oC, all specimens fractured in a complete ductile mode, showing the upper-shelf characteristic. Fig. 11 shows the fracture surface of a CT specimen broken at -30^oC. It can be seen that there is a transition form ductile tearing to cleavage. Also, a single trigger site for cleavage can be found in the fracture surface. According to the research of Ritchie et al [6], cleavage fracture criterion was postulated as opening stress exceeding cleavage stress σ_f over a microstructurally significant distance. Initially, Ritchie, Knott and Rice [6] assumed that the characteristic distance was two grain diameters. But in subsequent studies, Curry and Knott [29-30] found that no single relationship existed between grain size and characteristic distance and a statistical argument was introduced to explain the variation of the characteristic distance. In the present study, from the observation of fracture surfaces of CT specimens at -70^oC and -30^oC, there was a big scatter of the distance (X_f) from cleavage initiation site to the blunting or growing crack tip. The distance X_f ranges from 209~350 um at -70^oC and 188~1100 um at -30^oC, respectively. Similar phenomenon was also found in the work of Chen et al [31-32]. Therefore, for both stationary and growing cracks, the cleavage characteristic distance can be identified as a statistical distance needed to sample an eligible brittle particle. In this study, from the calculated stress distribution corresponding to the fracture load, the opening stress at the initiation site could be determined and was taken as the local stress needed to initiate cleavage fracture, i.e., σ_f, as described in Refs 31-32. The σ_f was measured at -70^oC and -30^oC and temperature basically has no effect on σ_f. Also, no significant difference for σ_f

can be found for the specimens fractured with and without ductile growth. The lower bound σ_f is 1081MPa and the average value is 1167MPa (out of 13 specimens).

In Fig. 8, the peak opening stress remains almost constant after a small amount of ductile growth. With the assumption of σ_f being insensitive to constraint level, the possibility of cleavage fracture after some amount of ductile growth, i.e., ductile-brittle fracture transition, can be approximately predicted by comparing the calculated peak opening stress with the measured cleavage stress σ_f.

Table 4 shows the peak opening stress achievable for the specimens during crack blunting (stationary crack) and subsequent ductile growth at 30^{o}C. From Table 4, it is clear that even the peak opening stress ahead of a growing crack tip for M(T) and SE(B) is lower than the low bound σ_f . As a result, at this temperature cleavage cannot occur and fracture shows a complete ductile tearing. This is in agreement with the experimental results at 30^{o}C at which no cleavage fracture has been found for M(T) and SE(B) specimens [11]. On the other hand, for CT specimen the peak opening stress ahead of the stationary crack is below σ_f but the stress exceeds σ_f after ductile growth. This means that cleavage can occur after some ductile crack growth. This is in agreement with the experimental result at 30^{o}C at which ductile-brittle transition occurred after some crack growth. Therefore, in-plane constraint affects the magnitude of opening stress ahead of both stationary and growing cracks, which in turn affects the ductile-brittle fracture transition.

For carbon steel, the yield stress σ_o is dependent on test temperature (Table 2) and the absolute magnitude of opening stress ahead of crack tip changes with temperature. Fig. 12 shows the peak opening stress achievable ahead of the stationary and growing crack

tips. The peak opening stress increases with decreasing temperature. Fig. 12 also shows the low bound σ_f (1081MPa). At about 5^{o}C, the peak stress ahead of the stationary crack just approaches σ_f and it exceeds σ_f below 5^{o}C. This means that below 5^{o}C complete cleavage fracture can occur and fracture is in the low-shelf or lower-transition region. From 5^{o}C to 30^{o}C, the peak stress ahead of the stationary crack is lower than σ_f but its value exceeds σ_f after crack growth. This means that cleavage would invariably be preceded by ductile crack growth. Above 30^{o}C, even the peak stress ahead of the growing crack is lower than σ_f. Cleavage cannot occur above this temperature and fracture shows complete ductile tearing. These transition temperatures are basically in consistent with the experimental observation, as shown in Fig. 10.

5. Conclusions

Ductile-brittle fracture transition has been investigated using compact tension (CT) specimens from -70^{o}C to 40^{o}C. The stress and strain distributions ahead of stationary and growing cracks in compact tension (CT), three-point bend (SE(B)) and central-cracked tension (M(T)) specimens have been analyzed using finite element method. Both experimental and numerical results supported the following conclusions:

1. The ductile crack growth is sensitive to the in-plane constraint level. The tearing modulus of J-integral and crack tip opening displacement (CTOD) resistance curves and crack tip opening angle (CTOA) decrease with increasing constraint. The CTOA nearly

remains constant during ductile growth. Path-dependence of J-integral occurs from the very beginning of crack growth.

2. There was a large scatter of the distance from cleavage initiation site to the blunted and growing crack tips. Based on the finite element analysis and fracture surface observation, the local cleavage stress has been measured

3. After ductile growth, opening stress increase initially then remains stable in the remaining ligament. Effective plastic strain ahead of a growing crack falls significantly below the distribution for the stationary crack. Cleavage may occur after ductile crack growth due to the increase of opening stress.

4. For both stationary and growing cracks, the magnitude of opening stress increases with increasing constraint. The ductile-brittle fracture transition is due to the opening stress ahead of the crack tip reaching the cleavage stress as the constraint increases.

References

1. Atkins, A.G and Mai, Y.W., *Elastic and Plastic Fracture*, John Wiley/Ellis Horwood, Chichester, 1985
2. Knott, J.F., *Fundamentals of Fracture Mechanics*, Butterworths, London, 1973
3. Wu, S.X, Mai, Y.W. and Cotterell, B., *Acta Metallurgica Mater*. 39 (1991) 2527
4. O'Dowd, N.P and Shih, C.F., *Journal of Mechanics and physics of Solids* 39 (1991) 989-1015.
5. O'Dowd, N.P. and Shih, C.F., *Journal of Mechanics and physics of Solids* 40 (1992) 939-963.

6. Ritchie, R.O., Knott, J.F. and Rice, J.R., *Journal of Mechanics and physics of Solids* 21 (1973) 395-410.

7. O'Dowd, N.P. and Shih, C.F., in *Constraint Effect in Fracture: Theory and Applications*, ASTM STP 1244, Philadelphia (1994) 1-25.

8. A.G. Varias and C.F. Shih, *Journal of Mechanics and Physics of Solids* 41(1993) 835-861.

9. L. Xia, and C.F. Shih, *Journal of Mechanics and Physics of Solids* 44 (1996) 603-639.

10. C. Ruggieri and R.H. Dodds, Jr, *International Journal of Fracture* 79(1996) 309-340.

11. Wu, S.X., and Mai, Y.W., in *Fracture Mechanics: 26th Volume*, ASTM STP 1256, Philadelphia (1995) 43-53.

12. Hellmann, D. and Schewable, K.-H., in *The Crack Tip Opening Displacement in Elastic-Plastic Fracture Mechanics*, Springer-Verlag, (1986) 115-132.

13. Hibbitt, Karlsson and Sorensen, Inc., *ABAQUS user's and Theory Manual*, Version 5.5. Providence (1996)

14. Brocks, W. and Yuan, H., *Engineering Fracture Mechanics* 32(1989) 459-468.

15. Newman, J.C, Booth, B.C. and Shivakumar, K.N., in *Fracture Mechanics: 18th Symposium*, ASTM STP 945, Philadelphia (1988) 665-685.

16. ASTM E1152-95, *Annual Book of ASTM Standards*, Vol. 03.01, Philadelphia (1996) 750-763.

17. J. W. Hutchinson, *Journal of Mechanics and Physics of Solids* 16 (1968) 13-31

18. J. R. Rice, G. F. Rosengren, *Journal of Mechanics and Physics of Solids* 16 (1968) 1-12.

19. Hutchinson, J.W., and Paris, P.C., in *Elastic-Plastic Fracture*, ASTM STP 668, Philadelphia (1979)37-64.

20. Shih, C.F. and German, M.D., *International Journal of Fracture* 17(1981) 27-43.

21. Gibson, G.P., Druce, S.G. and Tuner, C.E., *International Journal of Fracture* 32(1987) 219-240.

22. Brocks, W and Schmitt, W., in *Constraint Effects in Fracture: Theory and Applications*, ASTM STP 1244, Philadelphia (1995) 209-231.

23. Roos, E., Eisele., U. and Silcher, H., in *Constraint Effect in Fracture*, ASTM STP 1171, Philadelphia (1993) 41-63.

24. Bloom, J.R., Lee, D.R. and Van Der Sluys, W.A., in *Constraint Effect in Fracture*, ASTM STP 1171, Philadelphia (1993) 383-417.

25. Joyce, J.A., and Link, R.E., in *Fracture Mechanics: 26th Volume*, ASTM STP 1256, Philadelphia (1995) 142-177.

26. Xin, X.J., and Goldthorpe, M.R., *Fatigue and Fracture of Engineering Materials and Structure* 16 (1993) 1309-1327.

27. Sattari-Far, I., *Fatigue and Fracture of Engineering Materials and Structures* 18(1995) 1051-1069.

28. Lantridou, J.C., and Pineau, A., *International Journal of Fracture* 17(1981) R115-R119.

29. Curry, D. and Knott, J.F., *Metal Science* 13(1979) 341-345.

30. Curry, D. and Knott, J.F., *Metal Science* 14(1980)319-326.

31. Chen, J.H., G.Z. Wang, Z. Wang, L. Zhu, and Y.Y. Gao., *Metallurgical Transactions* 22A (1991) 2287-2296.

32. Chen, J.H., Yan, C. and Sun, J., *Acta Metallurgical and Materials* 42 (1994) 251-261.

33. Lewandowski, J.J., and Thompson, A.W., *Acta Metallurgica* 35 (1987) 1453-1462.

Table 1. Chemical composition of carbon steel (%)

C	Mn	Si	P	S
0.25	0.82	0.21	0.005	0.03

Table. 2 Yield strength & hardening exponent

Temperature(^{o}C)	Yield Strength (MPa)	Hardening Exponent	Constant K
-70	322	0.24	1066.1
-50	296	0.25	943.3
-30	278	0.25	908.2
0	250	0.25	904
10	243	0.23	769
20	236	0.23	715
30	226	0.23	662

Table. 3 Parameters associated with J-controlled crack growth

Specimen	Δa (mm)	$\Delta a/b_o$	$b\sigma_o/J_{12}$	ω
CT	0	0	79.4	256
	0.2	0.010	24.1	61.2
	0.3	0.015	22.4	16.5
	0.5	0.025	17.4	15.3
	1.0	0.050	12.2	12.7
	1.2	0.060	10.8	11.4
	1.3	0.065	9.62	10.5
SE(B)	0	0	53.0	810.9
	0.1	0.004	21.5	244.1
	0.8	0.035	8.2	19.7
	1.2	0.053	6.9	10.0
	1.3	0.060	6.4	8.8

Table. 4 The peak opening stress the specimens experienced

Specimens	σ_{max}, MPa (stationary crack)	σ_{max}, MPa (growing crack)
CT	994	1175
SE(B)	920	1062
M(T)	879	1037

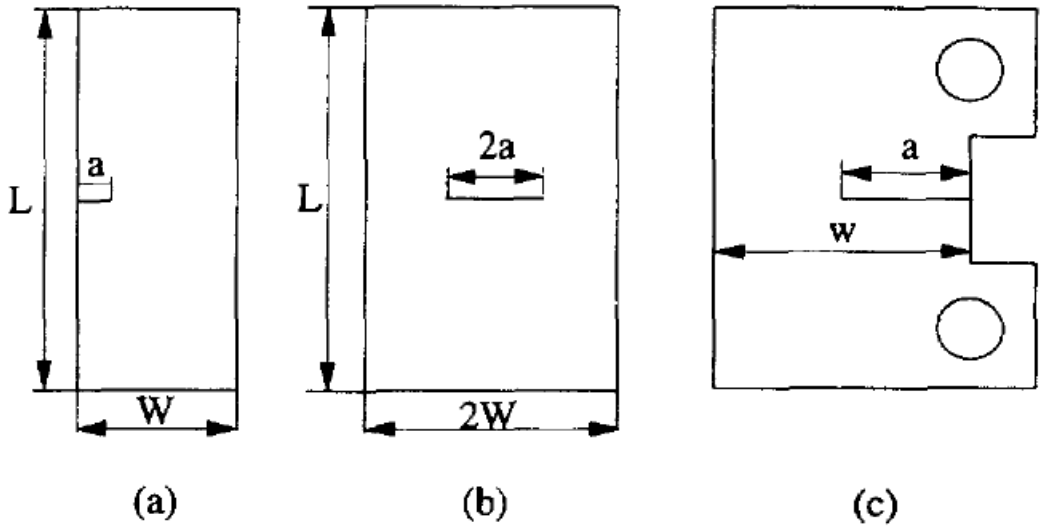

Fig. 1 (a) Three-point bend [SE(B)] specimen, L=130mm, W=25mm, and a=2.5mm, (b) centre-cracked tension [M(T)] specimen, L=300mm, W=25mm, and a=12.5mm, and (c) compact tension (CT) specimen, W=50mm, and a=30mm.

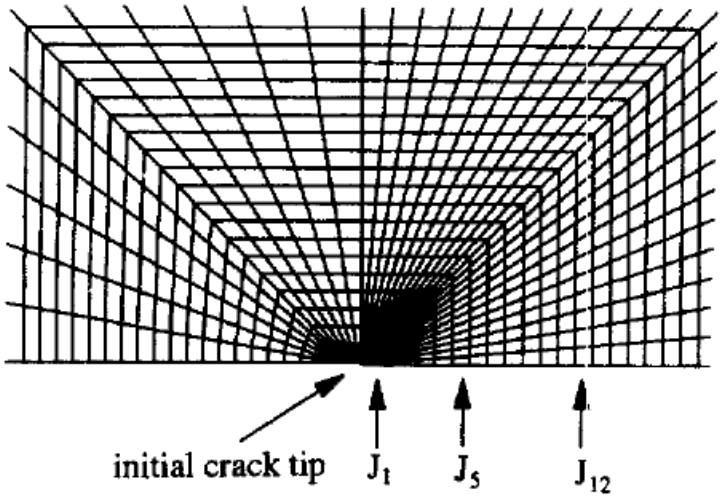

Fig. 2 Refined mesh for crack tip.

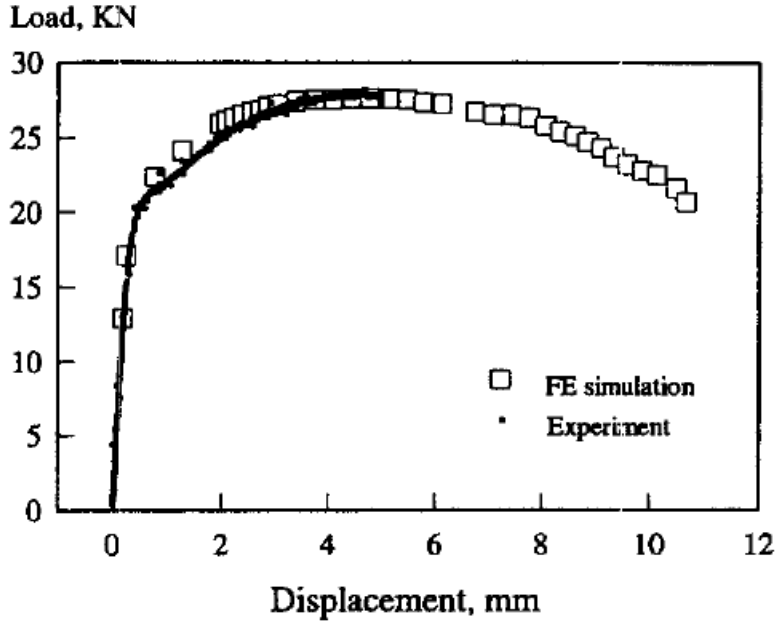

Fig. 3 δ_R-curves for CT, SE(B) and M(T) specimens.

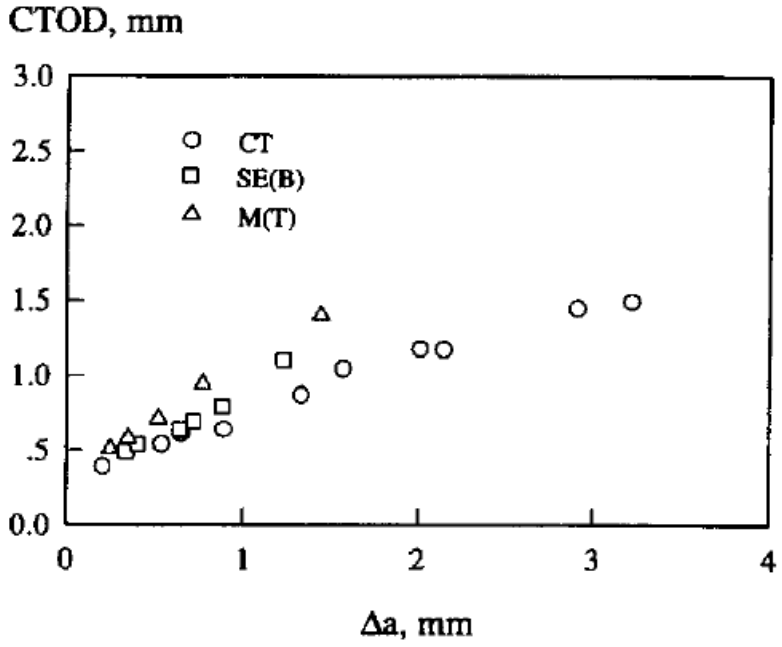

Fig. 4 Calculated load-load line displacement together with experimental record.

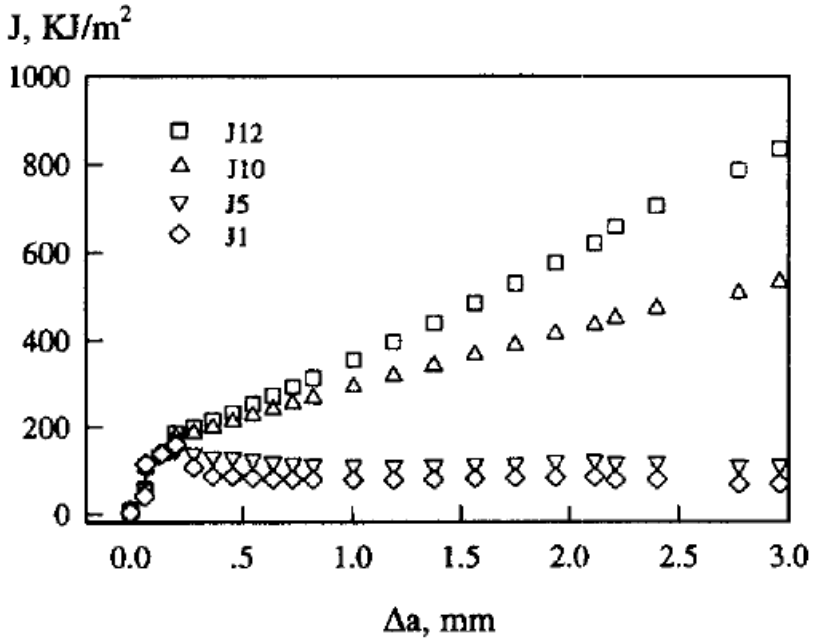

Fig. 5 J_R-curve calculated from different contours in CT specimen.

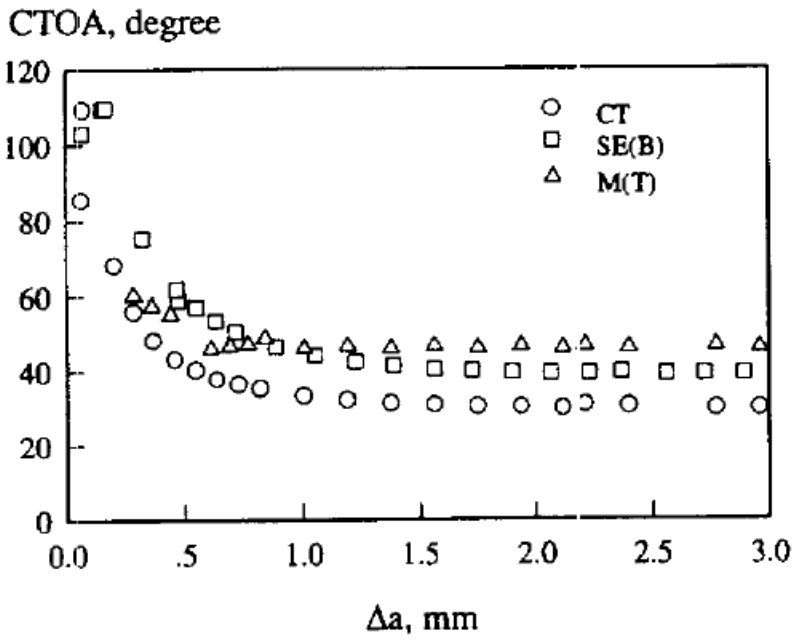

Fig. 6 Evolution of CTOA with crack growth.

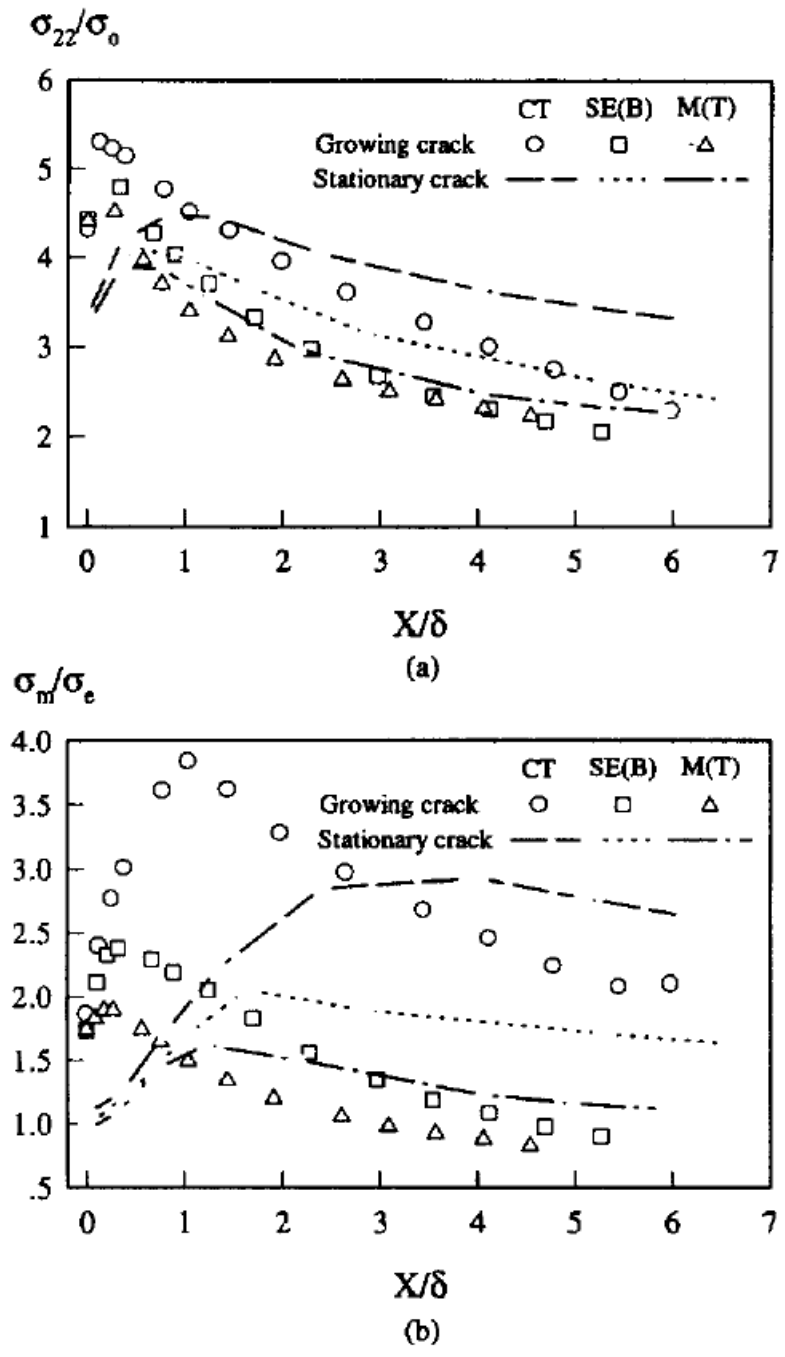

Fig. 7 Distributions of (a) opening stress σ_{22}/σ_o, and (b) stress triaxiality σ_m/σ_e.

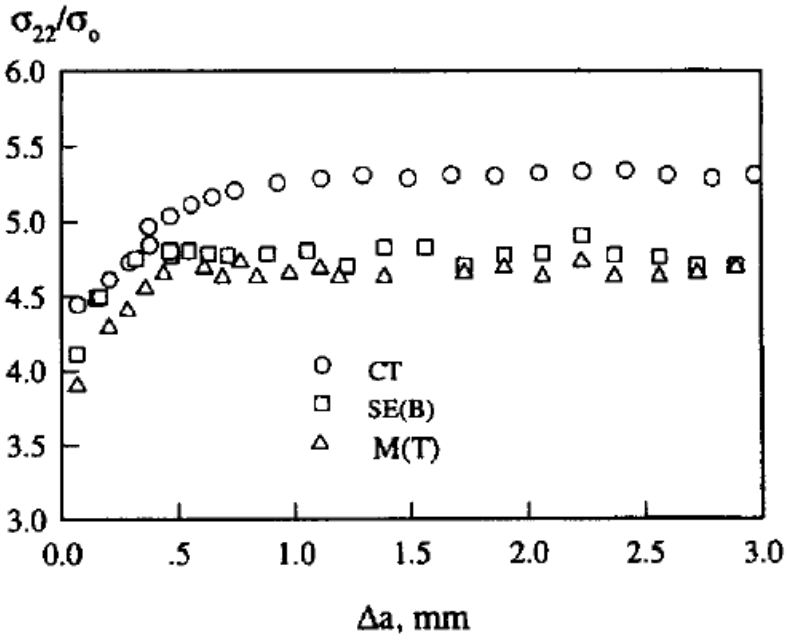

Fig. 8 Variation of peak opening stress with crack growth.

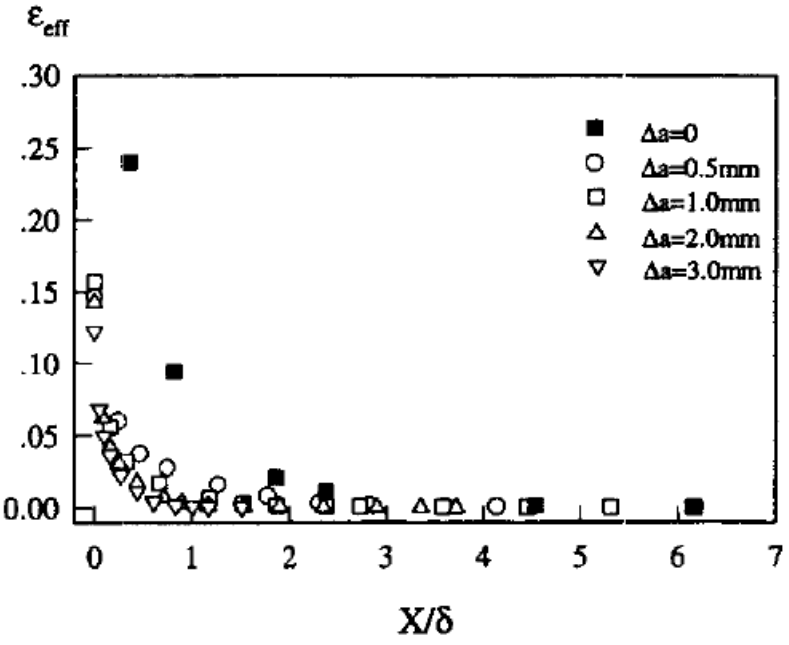

Fig. 9 Distribution of effective plastic strain at different stages of crack growth.

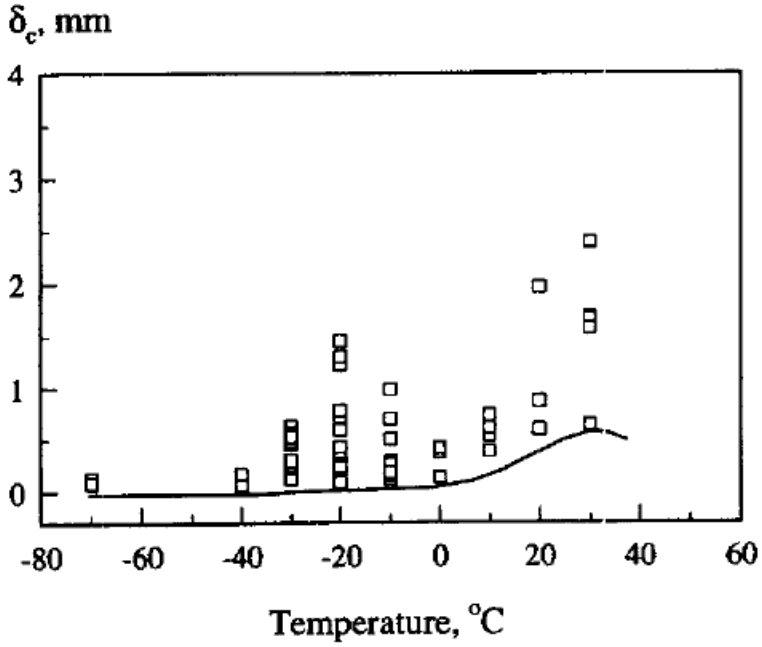

Fig. 10 Variation of CTOD (δ_c) with temperature.

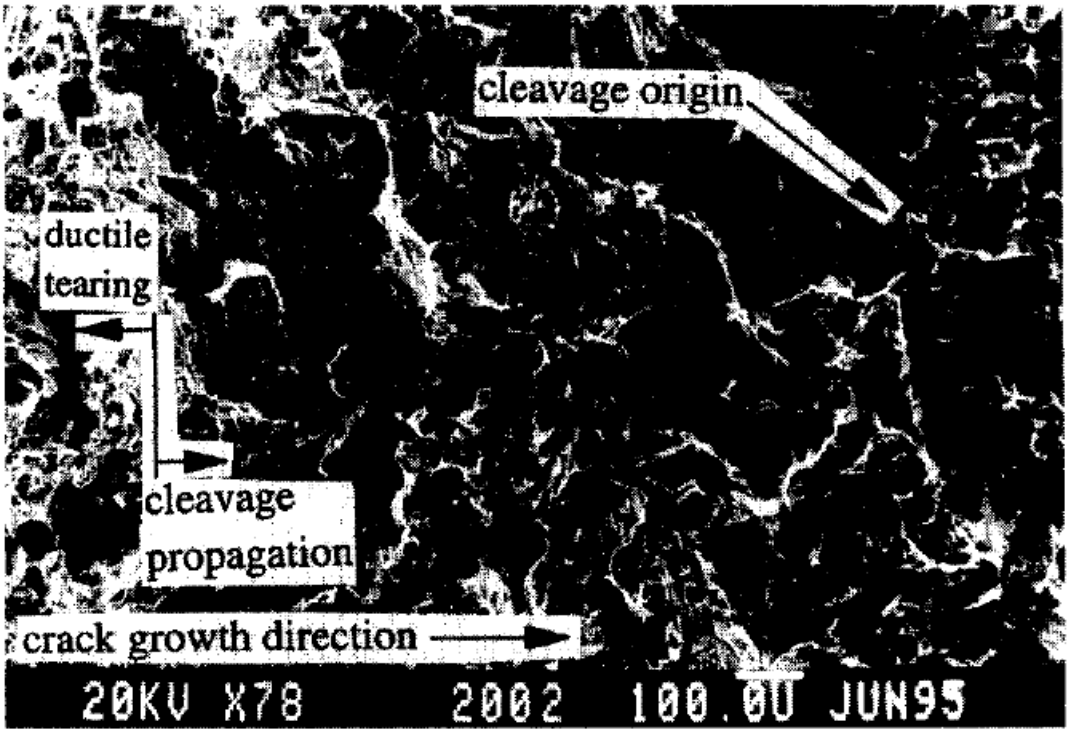

Fig. 11 Fracture surface of CT specimen at -30°C.

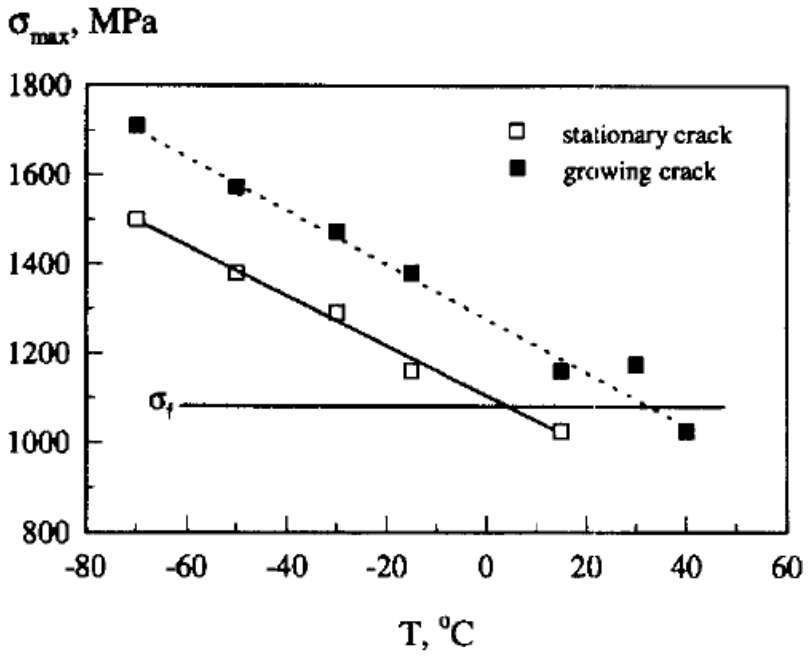

Fig. 12 Prediction of ductile-brittle transition at different temperatures.